tvst

Article

Microporous Drug Delivery System for Sustained Anti-VEGF Delivery to the Eye

Chengxin Zhou[1,2], Arushi Singh[1], Grace Qian[1], Natalie Wolkow[2,3], Claes H. Dohlman[1,2], Demetrios G. Vavvas[5], James Chodosh[1,2,4], and Eleftherios I. Paschalis[1,2,4]

[1] Boston Keratoprosthesis Laboratory, Department of Ophthalmology, Massachusetts Eye and Ear and Schepens Eye Research Institute, Boston, MA, USA
[2] Harvard Medical School, Boston, MA, USA
[3] David G. Cogan Laboratory of Eye Pathology and Ophthalmic Plastic Surgery Service, Massachusetts Eye and Ear Infirmary, Boston, MA, USA
[4] Disruptive Technology Laboratory (D.T.L.), Massachusetts Eye and Ear, Department of Ophthalmology, Harvard Medical School, Boston, MA, USA
[5] Angiogenesis Laboratory, Retina Service, Department of Ophthalmology, Massachusetts Eye and Ear Infirmary, Harvard Medical School, Boston, MA, USA

Correspondence: Eleftherios I. Paschalis, Department of Ophthalmology, Boston Keratoprosthesis Laboratory, Massachusetts Eye and Ear Infirmary and Schepens Eye Research Institute, Harvard Medical School, Boston, MA 02114, USA. e-mail: eleftherios_paschalis@meei.harvard.edu

Received: January 27, 2020
Accepted: May 4, 2020
Published: July 2, 2020

Keywords: neovascularization; cornea; VEGF; avastin; bevacizumab; angiogenesis; inflammation; retina

Citation: Zhou C, Singh A, Qian G, Wolkow N, Dohlman CH, Vavvas DG, Chodosh J, Paschalis EI. Microporous drug delivery system for sustained Anti-VEGF delivery to the eye. Trans Vis Sci Tech. 2020;9(8):5, https://doi.org/10.1167/tvst.9.8.5

Purpose: To describe a novel microporous drug delivery system (DDS) for sustained anti-vascular endothelial growth factor (VEGF) delivery to the eye and to evaluate its efficacy in a corneal injury model.

Methods: A macro-porous DDS (1.5 × 1.5 × 4 mm) loaded with 2 mg of bevacizumab was implanted subconjunctivally in three Dutch-belted pigmented rabbits after corneal alkali injury (2N NaOH). Three rabbits received sham DDS. Animals were followed for three months and assessed in vivo and ex vivo for corneal neovascularization (NV), epithelial defect, stromal scarring, endothelial cell loss, and expression of angiogenic and inflammatory markers in the cornea and retina.

Results: Anti-VEGF DDS treatment led to complete inhibition of superior cornea NV and complete corneal re-epithelialization by day 58 whereas sham DDS resulted in severe cornea NV and persistent epithelial defect (9%∼12% of total cornea area) through the end of the study. Histologically, anti-VEGF DDS significantly reduced $CD45^+$ and F4/80 $CD11b^+$ cell accumulation (79%, $P < 0.05$) in the cornea, ameliorated tumor necrosis factor–α expression (90%, $P < 0.05$), reduced corneal stromal scarring and prevented corneal endothelial cell loss, as compared to sham DDS. Moreover, anti-VEGF DDS achieved retinal penetration and reduction in retinal VEGF levels at 3 months.

Conclusions: Use of subconjunctival anti-VEGF DDS suppresses cornea NV, inflammation, stromal scarring, prevents endothelial cell loss, and abrogates retinal VEGF upregulation in a rabbit corneal alkali burn model. Moreover, it delivers anti-VEGF antibodies to the retina for three months. This delivery platform could enable antibody therapy of other corneal and retinal vascular pathologies.

Translational Relevance: We describe a method for sustained anti-VEGF delivery to the eye for the treatment of ocular injuries.

Introduction

Severe ocular injury, hypoxia, infection, inflammation or trauma frequently lead to corneal neovascularization (NV) and blindness, affecting approximately 1.4 million people per year.[1] A key regulator of corneal NV is vascular endothelial growth factor (VEGF) which becomes upregulated after the insult.[2,3] Once deep corneal stromal vessels are established, subsequent surgical rehabilitation of the cornea becomes more difficult.[4,5] Recent studies have shown that reducing the

degree of corneal neovascularization helps suppress the immunoinflammatory response after corneal surgery and improves graft survival.[1,2]

Most current therapies for corneal NV rely on the administration of corticosteroids and nonsteroidal anti-inflammatory eye drops, both associated with poor clinical outcomes.[6–8] More recently, VEGF inhibitors were proposed for the treatment of corneal NV[1,2,9–12] showing efficacy in experimental animal models,[13-15] as well as in clinical trials.[9–11] However, drug administration to the cornea has been a major issue; topical instillation requires increased anti-VEGF drug concentration to overcome poor drug penetration and bioavailability, which can lead to local toxicity.[2] In contrast, subconjunctival administration of VEGF inhibitor is more effective in terms of drug penetration[16,17] but still requires increased dosing to overcome rapid clearance.[18] Likewise, frequent intravitreal injections of anti-VEGF agents have become the gold standard for the treatment of retinal vascular pathologies.[19] Devising a minimally invasive method of antibody delivery to the intraocular tissues could improve the practicality and safety of the such therapies and possibly extend it to other ocular diseases, such as uveitis. To this end, we developed a novel drug delivery system (DDS) that allows sustained, low-dose, subconjunctival administration of antibodies to the eye for months.[20,21] This method allows a 50- to 100-fold reduction of the required therapeutic dose, as compared with subconjunctival anti-VEGF injection.

In this study we evaluate the therapeutic efficacy of an optimized version of the DDS, loaded with 2 mg of bevacizumab, for the treatment of corneal NV after severe corneal injury.[22] Furthermore, we evaluate the therapeutic efficacy of this treatment in reducing long-term corneal inflammation and promoting corneal re-epithelialization. Last, we investigate the ability of the subconjunctivally implanted DDS to deliver anti-VEGF to the retina and its efficacy in neutralizing retinal VEGF over three months.

Materials and Methods

Colloidal Crystal Templating and Characterization

A three-dimensional porous dolydimethylsiloxane (PDMS) scaffold was fabricated using colloidal crystal (CC) templating, resulting in crystallike interconnected porosity within the PDMS. To achieve this, poly(methyl methacrylate) (PMMA) microspheres of 100 ± 10 µm diameter (CorSpheric, CA, USA) were used as a temporary scaffold for the porous PDMS. PMMA spheres were washed with pure ethanol and centrifuged to remove small debris. Then, they were redispersed in fresh pure ethanol and allowed to settle overnight until sedimentation. The bead sediment was centrifuged at 10,000 rpm for 10 minutes, followed by ethanol evaporation at 40°C for two days. After that, dried PMMA spheres were annealed at 120°C for two days to bond adjacent spheres into a highly packed arrangement. The arrangement of the three-dimensional CC template was characterized using scanning electron microscopy. First the CC template was first desiccated using the Autosamdri 795 Supercritical Point Dryer (Tousimis, Rockville, MD, USA), mounted on aluminum specimen holders, and sputter coated with a chromium ion beam coater (model 681; Gatan, Pleasanton, CA). Sputtered CCs were imaged with a field emission scanning electron microscope (JSM-7401F; Jeol Ltd., Tokyo, Japan) at magnification ×100 and ×250.

DDS Fabrication and evaluation of porosity

The porous PDMS scaffold was fabricated using previously published techniques.[20,23] Briefly, PDMS elastomer was mixed with the curing agent (7:1 w/w) and infiltrated into the CC template in vacuum chamber for 2 hours. The composite was cured overnight at 65°C followed by CC removal using pure acetone for 2 days and repeated washing in pure ethanol. Porous PDMS sections (1.5 × 1.5 × 4 mm; length × width × height) were prepared as drug carriers. The porosity of the DDS was evaluated using three-dimensional x-ray micro-computed-tomography (µCT) (X-Tek HMXST225; Nikon Metrology Inc., Brighton, MI, USA) and three-dimensional image rendering (VGStudio Max 2.2, Heidelberg, Germany), as described previously.[21]

Antibody Loading Into the DDS

Bevacizumab solution (25mg/mL) was lyophilized in a freeze dryer (FreeZone 4.5L -84C; Labconco, Kansas City, MO, USA). Lyophilized bevacizumab powder was dissolved in 10% (w/v) polyvinyl alcohol (PVA) and infused into the porous PDMS segment using a vacuum for two hours. Anti-VEGF DDS was air-dried, gamma-radiated (25 kGy) for sterilization, and stored at 4°C until use.

Drug release characterization (in vitro)

Drug release kinetics were evaluated using fluorescein-dextran as a substitute for bevacizumab.

Both agents have a similar molecular weight (150 kDa),[24] thereby allowing reliable approximation of drug release. DDSs (0.03∼0.05 g total weight) loaded with 10% PVA containing 2.5% w/v fluorescein-dextran were submerged separately in 1.5 mL Eppendorf tubes containing 750µL of phosphate-buffered solution (PBS) and incubated for 48 hours at 37°C protected from light. Each DDS was transferred to a new vial with fresh 750 µL of PBS every second day for one month. Supernatant was stored at 4°C in the dark for fluorescein intensity measurements using a 96-well microplate reader with excitation at 488 nm. All measurements were performed in triplicate. The relative fluorescence intensity was converted to fluorescein-dextran concentration through a standard curve. The total amount of fluorescein-dextran in 750 µL supernatant was normalized by the total weight of the DDS and the days of incubation to yield a metric of drug release quantity in µg/day/1 g of DDS. The cumulative fluorescein-dextran release (as a percentage of total drug amount in each DDS) was quantified as a function of time.

Corneal NV Model

Corneal alkali burn was used to generate corneal NV.[21,22,25,26] All rabbits were treated in accordance with the Association for Research in Vision and Ophthalmology Statement on the Use of Animals in Ophthalmic and Vision Research and the National Institutes of Health guide for the care and use of Laboratory animals, and the experimental protocol was approved by the Animal Care Committee of the Massachusetts Eye and Ear. Six female Dutch-Belted rabbits (2–2.5 kg), (Covance, Dedham, MA, USA) were anesthetized by intramuscular injection of ketamine hydrochloride INJ, USP (35 mg/kg; KetaVed; VEDCO, St. Joseph, MO, USA) and xylazine (5 mg/kg; AnaSed, LLOYD, Shenandoah, IA, USA). Topical anesthetic (0.5% proparacaine hydrochloride; Bausch & Lomb, Tampa, FL, USA) was applied to the eye. Alkali burn was performed using an 8-mm diameter cotton sponge soaked in 2N NaOH, applied to the cornea for 20 seconds. The eye was immediately irrigated with saline solution for 15 minutes.

Subconjunctival DDS Placement

DDSs loaded either with 2 mg of bevacizumab ($n = 3$) or immunoglobulin G (IgG) control ($n = 3$) (1.5 × 1.5 × 4 mm; length × width × height, 20 mg in total weight) were placed subconjunctivally immediately after the corneal burn. Implantation was performed in the inferior bulbar conjunctiva to avoid dislocation of the polymer. A narrow lateral subconjunctival pocket (4 mm in length) was created using fine spring surgical scissors. The DDS was inserted into the pocket, and the conjunctiva was sutured using three interrupted 8-0 polyglactin sutures. Erythromycin ophthalmic ointment (0.5%, Bausch & Lomb) was administered topically twice a day for one week.

Evaluation of Corneal NV and Re-Epithelialization

Evaluation of corneal NV was performed weekly for the first month and biweekly thereafter for two additional months under general anesthesia. Topical anesthetic 0.5% proparacaine hydrochloride was applied to the eye. All treated and control eyes were photographed using a digital SLR camera (Nikon, Tokyo, Japan) attached to a surgical microscope (S21; Carl Zeiss, Jena, Germany) at standard magnifications. Corneal epithelial defects were stained with fluorescein and imaged using a portable slit-lamp (Keeler 3010-P-2001; Keeler Americas, Malvern, PA, USA) equipped with cobalt blue filter and a mounted digital camera at magnification ×10. Photographs were analyzed using ImageJ 1.50e software (http://imagej.nih.gov/ij/; provided in the public domain by the National Institutes of Health [NIH], Bethesda, MD, USA). For epithelial defect, total corneal area with fluorescein stain ($pixel^2$) was normalized by the relative whole cornea area ($pixel^2$) in the same image, yielding the corneal epithelial defect area per whole cornea ratio (%). For CNV analysis, each cornea was divided into superior and inferior halves. The vascularized area in each half was quantified and normalized by half of the corneal area (%). The relative inhibition of CNV by anti-VEGF DDS treatment was also calculated for both the superior and inferior corneas. Relative percentage of CNV inhibition $= (Mean\%CNV_{sham} - Mean\%CNV_{anti\text{-}VEGF}) / Mean\%CNV_{sham} * 100$.

Histological and Immunohistochemical Evaluation of the Cornea

At three months, rabbits were euthanized using intravenous Beuthanasia-D (sodium pentobarbital and phenytoin sodium, 100 mg/kg; Merck Animal Health, Madison, NJ, USA). Tissues were fixated in 4% paraformaldehyde (PFA and embedded in optimal compound temperature (OCT). Tissue frozen sections (10 µm thickness) were prepared using a cryostat (CM1950; Leica Biosystems, Buffalo Grove, IL, USA).

Hematoxylin and eosin (H&E) staining was performed on methacrylate embedded tissue sections for histologic evaluation. Immunohistochemical evaluation was performed as previously described.[21] Primary antibodies diluted in 1% bovine serum albumin were incubated with the tissue samples overnight at 4°C, followed by secondary antibody incubation for two hours at room temperature. Detail information of the antibodies is provided in the Supplementary Methods section. Immune cell recruitment, cytokine expression, and lymphangiogenesis were assessed using antibodies against CD45, F4/80, CD11b, tumor necrosis factor–α (TNF-α), LYVE1 (Supplementary Methods). Residual bevacizumab in the DDS and in the ocular tissues was determined using goat anti-human IgG antibody (Thermo Scientific, Waltham, MA, USA). The total number and area of cells expressing TNF-α, VEGF-A, F4/80^{+}CD11b^{+}, and CD45, LYVE1 in corneal sections were determined using the "Analyze Particles" tool in ImageJ software, as previously described.[22] Mean ± standard deviation (SD) of three different rabbits were reported.

Results

Fabrication and Characterization of the Three-Dimensional Inverse Colloidal Crystal DDS Scaffold

Sedimentation-evaporation at 40°C led to self-assembly of 100 µm PMMA microspheres in a compact, coherent colloidal crystal (CC) arrangement, with face-centered cubic close packing (Fig. 1A). SEM analysis of the CC surface showed that PMMA microspheres were tightly ordered in a crystal form with small structural voids intermittently (Fig. 1B). CC blocks 20 mm in length, 12 mm in diameter, 0.15 g weight were fabricated as a temporary scaffold for inverse CC templating. To achieve this, the CC template was infiltrated with liquid PDMS prepolymer and cross-linked in situ, and PMMA spheres were leached out with acetone. This generated a highly ordered PDMS inverse scaffold, with a translucent, densely-packed foamy appearance (Figs. 1C, 1D). Using three-dimensional X-ray microtomography, we showed that PMMA template annealing resulted in PDMS porosity of 83% (Fig. 1E), higher than the potential maximum theoretical porosity of inverse opals from an ideally face-centered close-packed CC template (74%).[27] This was attributed to interdiffusion of adjacent spheres from annealing and the generation of frequent surface contact between adjacent PMMA spheres. Adjacent pores were interconnected, forming a continuous porous network (Fig. 1F). Cross-sectional slices (40 µm thickness) of the porous PDMS scaffold revealed numerous interconnections between adjacent spherical voids, reflecting the close contact between PMMA microspheres during CC templating (Fig. 1F: red arrows).

Drug Release Characterization Using Fluorescein Conjugated-Dextran In Vitro

To simulate the release kinetics of bevacizumab, we used fluorescein-conjugated dextran as a drug model for an in vitro release assay. Conjugated-dextran has similar molecular weight (150 KDa) to bevacizumab (Mwt = 149 KDa).[24] We observed burst FITC-dextran release within five days of DDS incubation in PBS at 37°C and subsequent normalization to first-order release over the course of 38 days (Figs. 2A, 2B). The initial burst of FITC-dextran release was 42% higher in the 100 µm pore size DDS compared with the 50 µm (Fig. 2B, "Day 3"). After burst release, the 100-µm DDS release rate was reduced by 74% and the 50-µm DDS by 42% at day 5 (Fig. 2B, "Day 5"). Both pore size DDSs exhibited first-order kinetics and provided sustained, long-term release of FITC-dextran over 38 days. The daily released dose was 0.36 µg/day (mean) at day 38 for both pore size DDSs, which exceeds the minimum bevacizumab dose that is required to achieve therapeutic outcome.[28,29]

Anti-VEGF Drug Present in the DDS 3 Months After Implantation

To investigate the presence of residual anti-VEGF monoclonal antibody (bevacizumab) in the DDS three months after implantation, we performed immunodetection of human IgG in explanted DDSs using anti-human IgG antibody. The DDS was retained in the subconjunctival space without complications for three months (Fig. 2C; black arrow). Explanation of the DDS at 3 months revealed that bevacizumab was still present within the device for further elution (Fig. 2D). In contrast, sham DDSs had no positive IgG signal (Fig. 2E).

Anti-VEGF DDS Inhibits Corneal Neovascularization After Corneal Alkali Burn

To determine the therapeutic efficacy of anti-VEGF DDS in corneal NV reduction, an established corneal NV model was used.[21,25,30] CNV analysis revealed that superior CNV was completely inhibited with anti-VEGF DDS throughout the study period (Figs. 3Q,

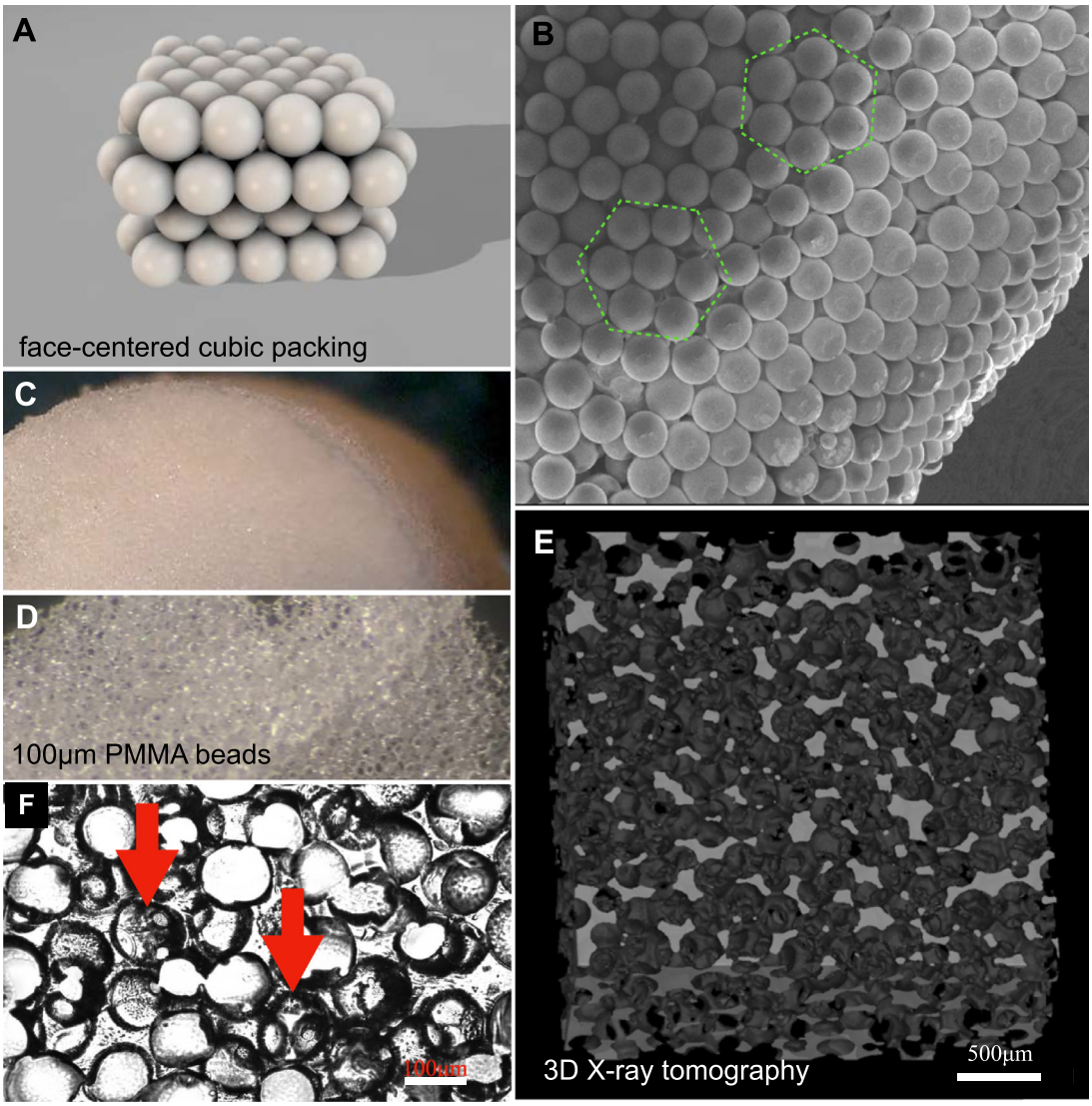

Figure 1. DDS scaffold structural characteristics. (A) schematic of theoretic face centered cubic packing of spherical particles. (B) A 100-µm PMMA bead colloidal crystal organization under scanning electron microscope. The beads appear tightly packed with hexagonal crystalline arrangement (dotted line). (C) Macroscopic image of the porous PDMS scaffold. (D) Bright field image ×20 of the porous PDMS scaffold. (E) A microCT three-dimensional radiographic image of a 100-µm bead PDMS scaffold. Scale bar = 500 µm. (F) Differential interference contrast microscopy ×25 of a thin section of the porous PDMS scaffold. Arrows indicate pore interconnectivity of adjacent voids which is the result of physical fusion of adjacent PMMA beads after annealing. Scale bar = 100 µm.

3S), ($P < 0.05$ mixed ANOVA). In contrast, sham DDS treatment led to marked and persistent CNV superiorly. Interestingly, inferior CNV was completely inhibited within the first 10 days by anti-VEGF DDS treatment (arrow; $P < 0.05$, two-tailed t-test) but evolved afterward, becoming similar to sham DDS treatment at two months (Figs. 3R, 3T) ($P > 0.05$ mixed ANOVA). Blood vessel growth and corneal NV were stabilized thereafter.

Biomicroscopic examination of sham DDS treated eyes revealed minimal peripheral corneal neovascularization within the first week (Figs. 3E, 3M), with new vessels emerging from the limbus at all clock hours within the first month (Figs. 3F, 3N). Thick major vessels were visible in sham DDS-treated eyes at day 30 as opposed to anti-VEGF DDS–treated eyes that exhibited fewer clock hours of corneal NV involvement and overall thinner vessels (Figs. 3B, 3J). Anti-VEGF DDS treatment was associated with reduced corneal stromal scarring and edema, and improved ocular surface quality, as compared with sham DDS–treated eyes at day 84 (Figs. 3D, 3H).

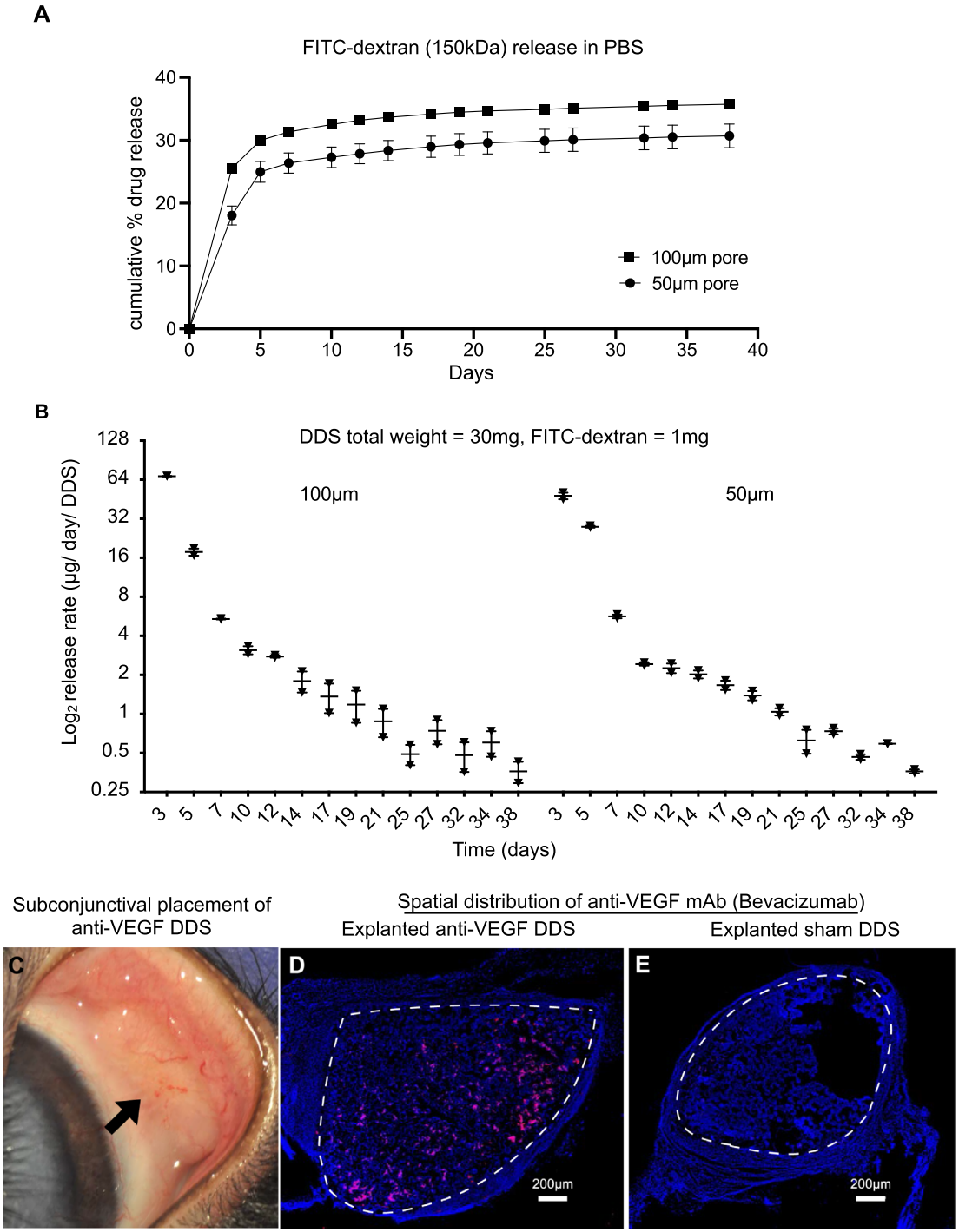

Figure 2. (A, B) In vitro release kinetics of 100 μm and 50 μm pore size DDSs eluting FITC-dextran (150 kDa) in PBS at 37°C for 38 days. A burst release is observed from both pore sizes during the initial 5 days of incubation. The 50-μm pore size DDS exhibits slower release rate than the 100-μm DDS, but both achieve first-order release kinetics in the subsequent incubation period (total 38 days). (A) Plot of percent cumulative FITC-dextran release versus time. (B) Log_2 release rate versus time. Each data point represents mean ± SD per incubation days of a 30-mg weight DDS releasing FTIC-dextran in PBS (n = 3/group). (C) A photograph of a rabbit eye showing the DDS under the conjunctiva three months after implantation (black arrow). (D, E) Remaining bevacizumab three months after DDS implantation. (D) Bevacizumab is detected within the DDS three months after subconjunctival implantation in the lower fornix of rabbits. (E) No anti-VEGF staining in explanted sham DDS.

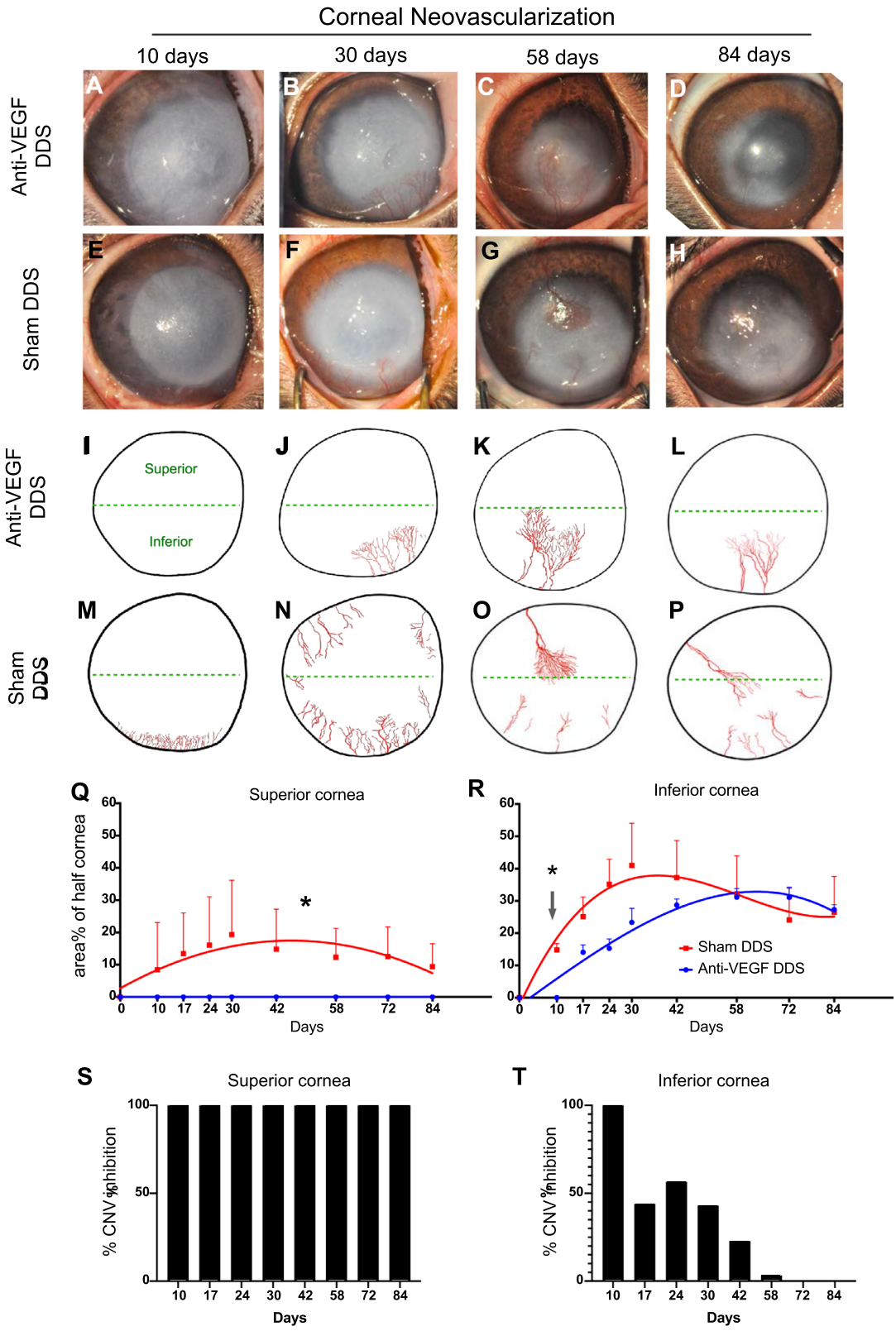

Figure 3. Corneal neovascularization after corneal alkali burn and treatment with anti-VEGF DDS. (A–D) Representative images of a burned eye, treated with anti-VEGF DDS at 10, 30, 60, and 90 days after the injury. (E–H) Representative images of a burned eye, treated with sham DDS (no drug) at 10, 30, 60, and 90 days after the injury. (I–L) Corneal angiographic reconstruction of anti-VEGF DDS and (M–P) sham DDS treated eyes at 10, 30, 60, and 90 days after the injury. (Q–R) Quantification of superior and inferior corneal neovascularization (NV) of anti-VEGF and sham DDS treated eyes showing complete elimination of superior corneal NV with anti-VEGF DDS treatment over three months

→

←

(Q: *$P < 0.05$; mixed ANOVA test) and complete inhibition of inferior corneal NV within the first 10 days (arrow in R: $P < 0.05$, unpaired *t*-test, two-tailed). After 10 days, comparison of inferior corneal NV between the two groups did not show statistical significance ($P > 0.05$; mixed ANOVA test). (S, T) Relative inhibition of cornea NV by Anti-VEGF DDS treatment in superior cornea (S) and inferior cornea (T). Relative percentage of cornea NV inhibition = (Mean%CNV_{sham} – Mean%$CNV_{anti\text{-}VEGF}$)/ Mean%CNV_{sham} *100.

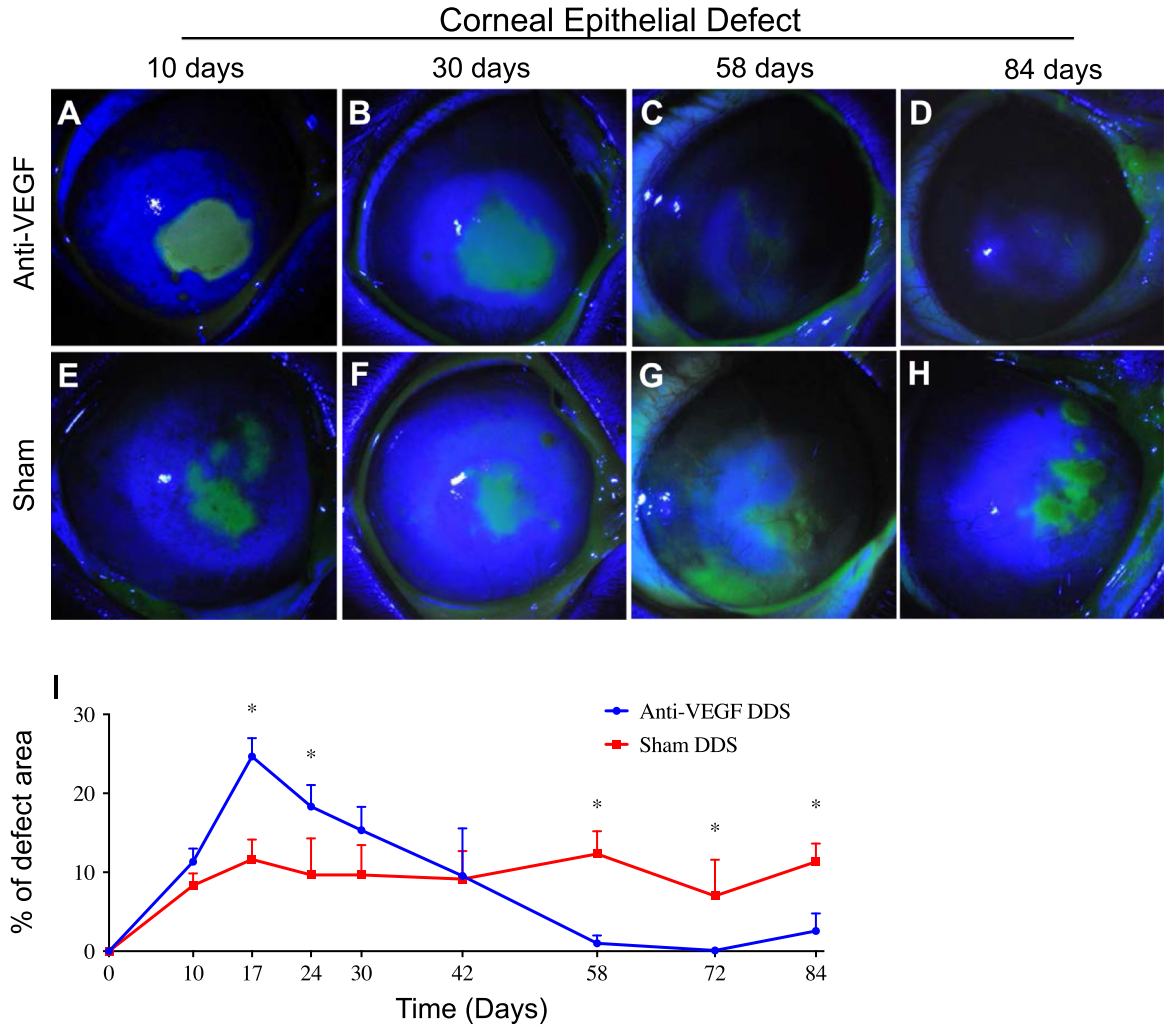

Figure 4. Corneal epithelial defect in anti-VEGF and sham DDS treated eyes. (A–H) Representative slit-lamp biomicroscopic images of fluorescein stained injured cornea 10 (A, E), 30 (B, F), 60 (C, G), and 90 days (D, H) after corneal alkali burn. (I) Anti-VEGF DDS treatment significantly promotes corneal re-epithelization as compared with sham DDS treatment. All corneas treated with anti-VEGF DDS exhibit significantly larger epithelial defect at day 17 and day 24, as compared with the sham DDS treated eyes. However, anti-VEGF DDS treated eyes begin to re-epithelialize near day 17, leading to completely re-epithelialization at day 72. Conversely, none of the sham DDS treated eyes achieves complete re-epithelialization by the end of the study. (*$P < 0.05$; unpaired *t*-test; n = 3).

Anti-VEGF DDS Treatment Improves Corneal Re-Epithelialization After Severe Eye Injury

The effect of anti-VEGF DDS treatment in corneal re-epithelialization after burn injury was assessed in vivo using serial fluorescein staining. Immediately after the injury, all corneas developed a similar 8-mm–diameter epithelial defect, which was equal to the diameter of the burn injury. Within the first 10 days, both the anti-VEGF– and sham DDS–treated eyes exhibited similar corneal epithelial defects of 10% of the surface (Figs. 4A, 4E, 4I). However, sham DDS–treated eyes retained this defect throughout the study period (84 days) (Figs. 4F, 4G, 4H, 4I), whereas anti-VEGF–treated eyes continued to improve, reaching complete re-epithelialization by day 58 (Figs. 4C, 4I), which was maintained until the end of the study (Figs. 4D, 4I).

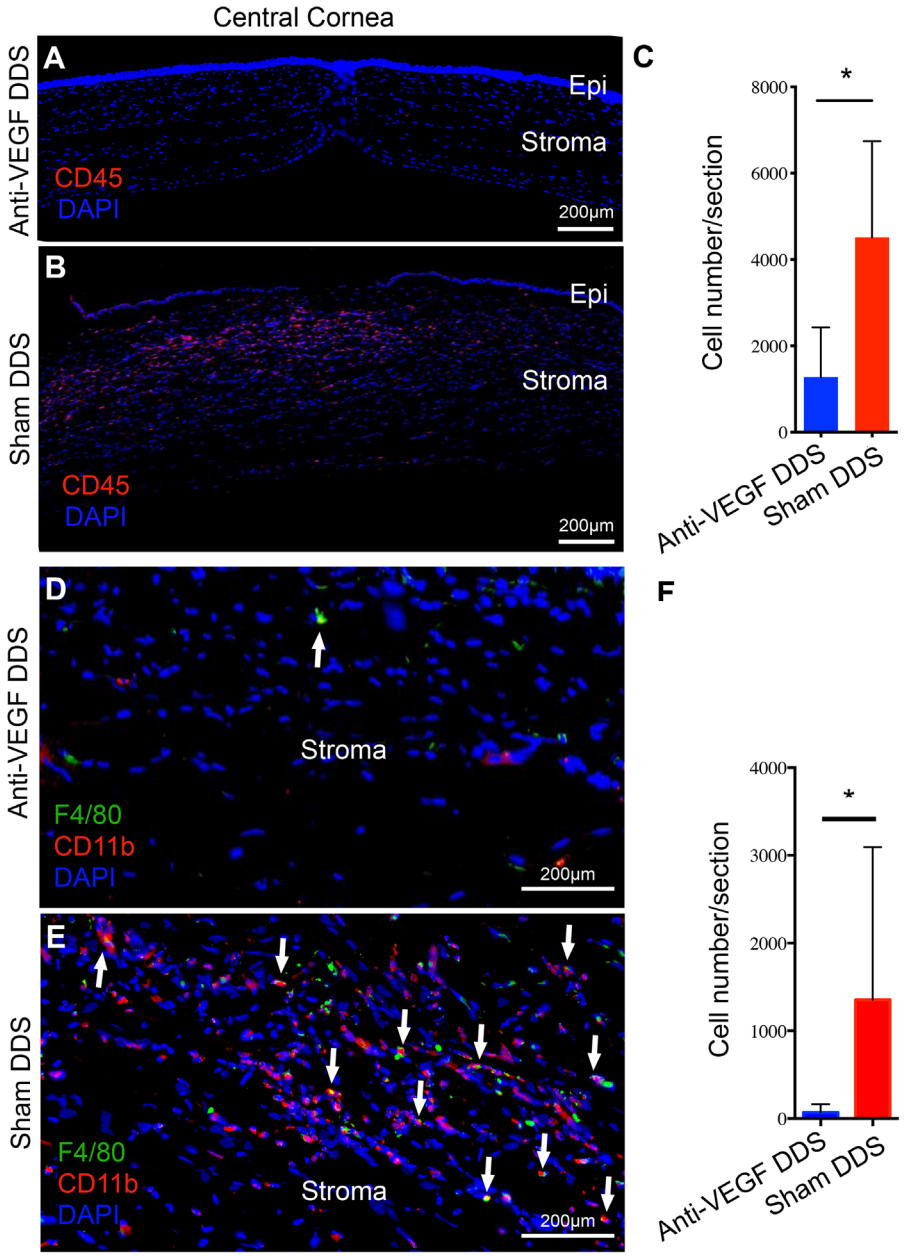

Figure 5. Effect of anti-VEGF DDS on inflammatory cell infiltration in the cornea. (A, B) Immunolocalization using anti-CD45 antibody in tissue sections shows that anti-VEGF DDS–treated eyes (A) exhibit reduced CD45 expression in the cornea, as compared with sham DDS–treated eyes (B). Quantification of $CD45^+$ corneal cell (C). Likewise, anti-VEGF DDS treatment suppress infiltration of $F4/80^+CD11b^+$ blood-derived macrophages in the burned cornea (D), as compared with sham DDS–treated eyes (E). Quantification of $F4/80^+$ $CD11b^+$ corneal macrophages (F). White arrows represent $F4/80^+$ $CD11b^+$ double-positive cells. Scale bar = 200 μm. (*$P < 0.05$; unpaired *t*-test; n = 3).

Anti-VEGF DDS Treatment Reduces Leukocyte Accumulation and TNF-α Expression in the Cornea

Tissue immunolocalization was performed using anti-CD45, F4/80, and CD11b antibodies three months after corneal injury to assess the effect of anti-VEGF DDS treatment on peripheral immune cell infiltration in the injured cornea. Anti-VEGF DDS treatment significantly reduced the number of $CD45^+$ cells in the cornea, as compared with sham DDS at three months ($P < 0.05$, unpaired *t*-test test), (Figs. 5A–5C). Further analysis showed a significant increase in the number of $CD11b^+$ $F4/80^+$ double positive

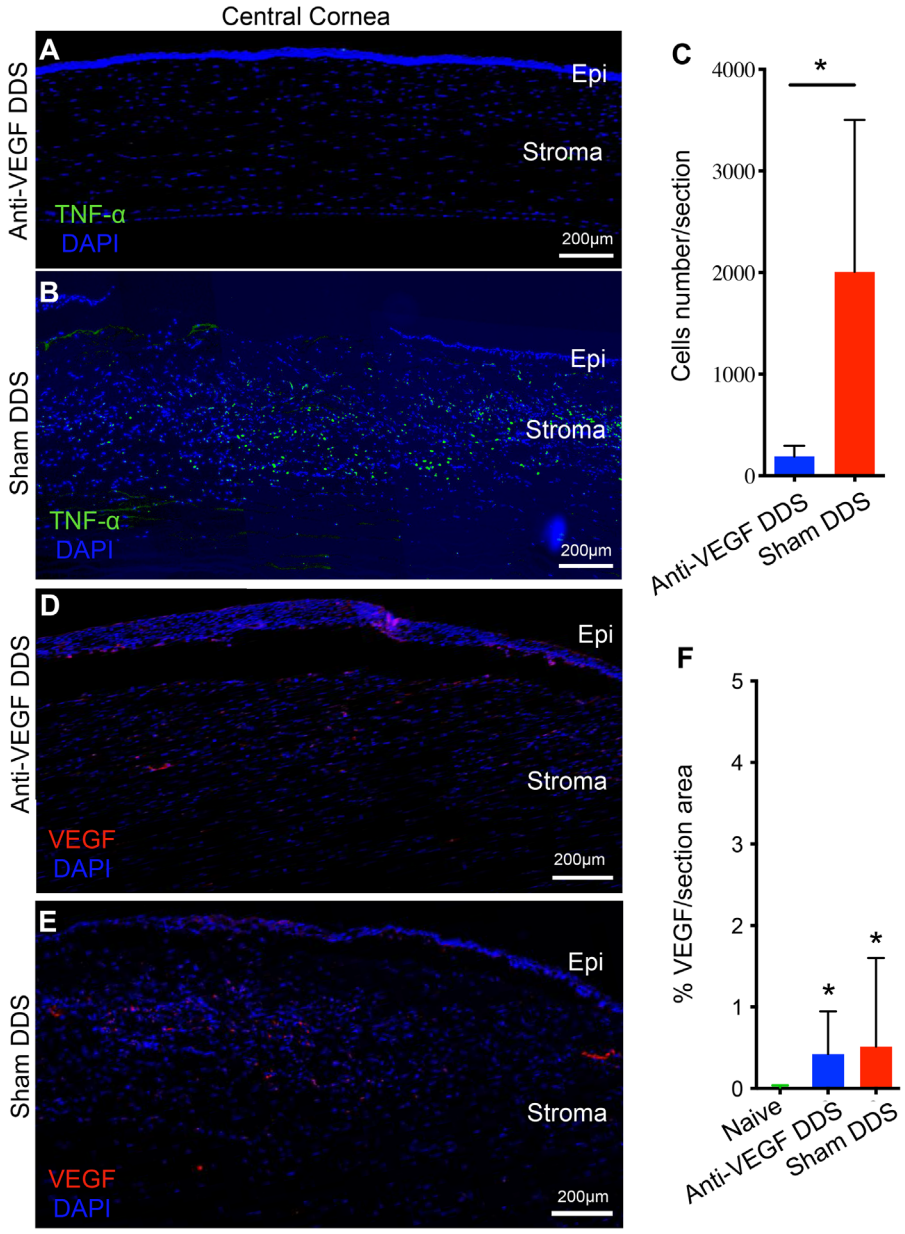

Figure 6. Effect of anti-VEGF DDS in TNF-α and VEGF expression in the cornea. (A–C) Immunolocalization using FITC-conjugated anti-TNF-α antibody in tissue sections of anti-VEGF DDS treated eyes (A) shows significant reduction (*$P < 0.01$; unpaired two-tailed *t*-test) of corneal TNF-α expression at three months, as compared with sham DDS–treated eyes (B). Quantification of corneal TNF-α expression at three months (C). (D–F) Corneal VEGF expression at three months. Quantification of corneal VEGF expression at 3 months (F), (*$P < 0.05$; unpaired two-tailed *t*-test compared to naïve rabbits; n = 3). (A–E) Scale bar = 200 μm.

macrophages in the corneas of sham DDS–treated eyes as compared with anti-VEGF DDS–treated eyes ($P < 0.05$, unpaired *t*-test), (Figs. 5D–5F). Likewise, TNF-α expression was significantly increased in the corneas of sham DDS–treated eyes, as compared with anti-VEGF DDS treated eyes ($P < 0.05$, unpaired *t*-test test), (Figs. 6A–6C). Three months after the burn, corneal VEGF-A expression in sham- and anti-VEGF DDS–treated eyes was elevated compared to naïve, (non-burned/non-DDS implanted) rabbits. No statistical difference, however, was present between the anti-VEGF– and sham DDS–treated groups ($P = 0.954$; Figs. 6D–6F). Likewise, anti-VEGF– and sham DDS–treated eyes exhibited similar LYVE1 expression in the corneal stroma at three months ($P > 0.05$; unpaired *t*-test; Supplementary Fig. S1).

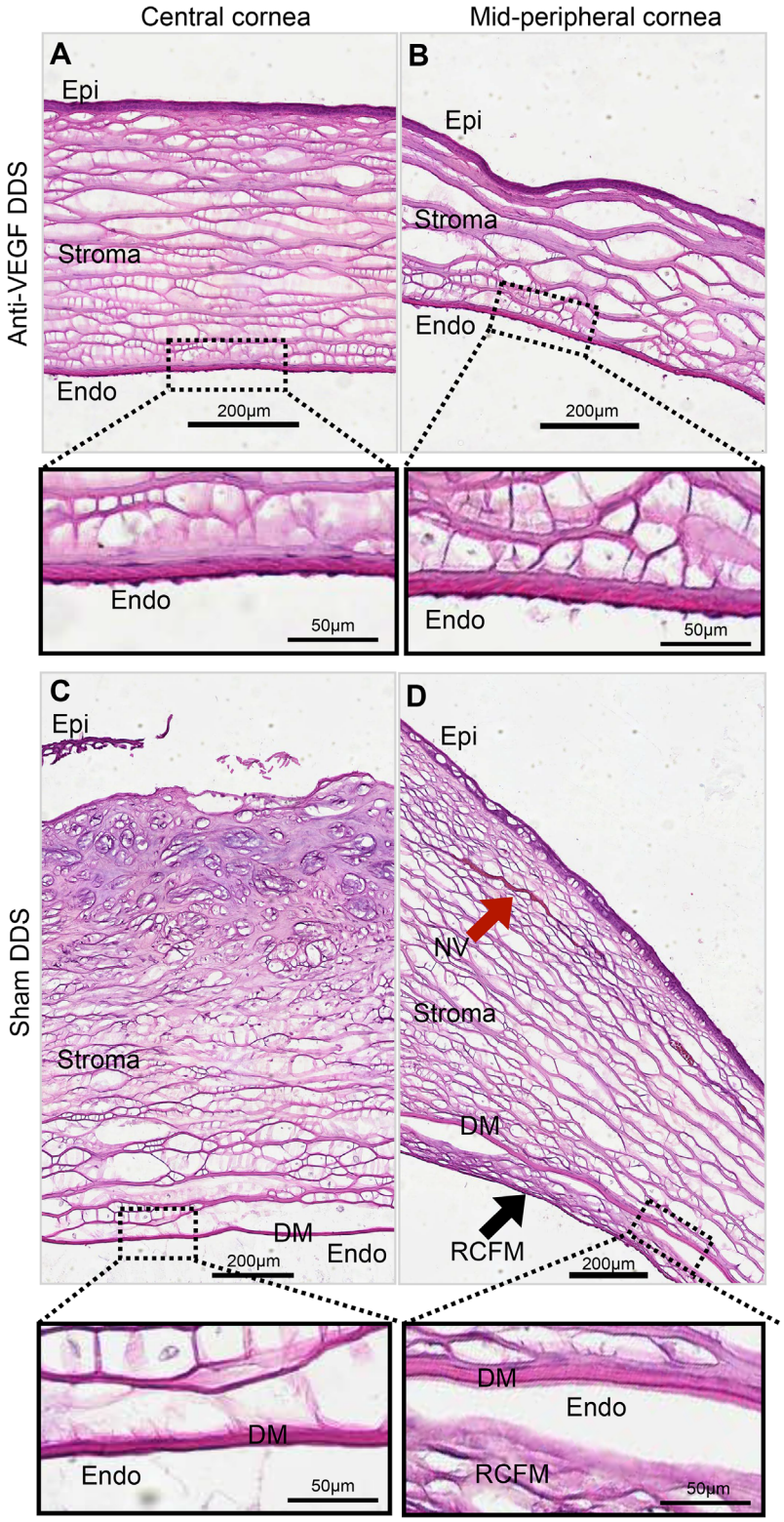

Figure 7. Anti-VEGF DDS treatment reduces corneal damage after burn injury and facilitates stromal wound healing. (A–D) Corneal H&E staining shows that anti-VEGF DDS treatment results improved corneal-epithelialization, mild anterior stromal scarring, and partial loss of endothelial cells at the center of the cornea (A). Anti-VGF DDS treated eyes exhibit improved peripheral corneal stromal morphology, normal endothelial cell distribution, and lack of retrocorneal membrane development (B). In contrast, sham DDS treatment exhibit significant epithelial thinning or absence of epithelium at the center of the cornea, severe stromal edema, thickening and scarring, and complete loss of endothelial cells (C). Moreover, peripheral cornea has large blood vessels and retrocorneal fibrous membrane (RCFM) (D, Red arrow points to neovascularization, black arrow points to RCFM). (A–D) Scale bar = 200 μm, insets = 50 μm.

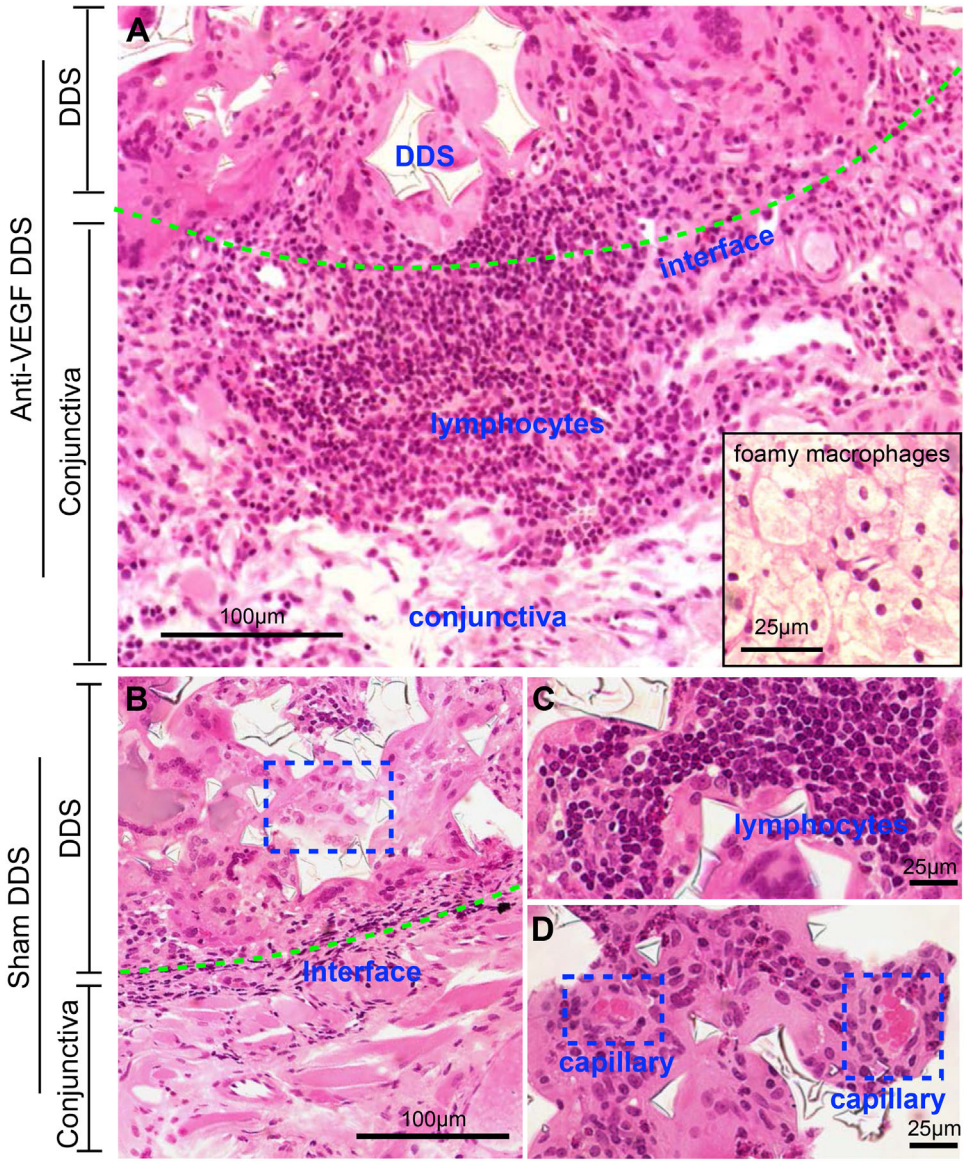

Figure 8. (A–D) H&E stains of methacrylate-embedded sections of explanted implant/tissue to assess the biological response of the DDS with the tissue. (A) Anti-VEGF DDS becomes infiltrated by different types of immune cells. Multinucleated giant cells are present within the pores of the DDS. A large population of lymphocyte aggregates is observed near the interface; this feature is less pronounced in the sham DDS (B). Inside the porous cavity, no capillaries are observed in the anti-VEGF DDS. Occasional foamy macrophages are observed in the host tissue surrounding the anti-VEGF DDS (insert, scar bar = 25 μm). (B–D) The sham DDS is mildly encapsulated by a thin collagenous membrane (B) and similar to the anti-VEGF DDS, the sham DDS is populated with multinucleated giant cells and occasional clusters of lymphocytes. Several lymphocyte clusters are present inside the sham DDS porous cavity (C, arrow), as well as small capillaries containing red blood cells (D). Scale bar in A, B = 100μm; scale bar in C, D, and the insert = 25 μm.

Histopathologic Analysis of Anti-VEGF and Sham DDS Treated Eyes After Burn

Further histopathologic analysis was performed with H&E staining. Anti-VEGF DDS–treated eyes had a normal corneal epithelium or minor corneal epithelial irregularities (thinning or thickening) centrally at the injury site. The peripheral cornea had normal epithelium (Figs. 7A, 7B). Moreover, anti-VEGF DDS–treated eyes showed minimal stromal scarring centrally at the site of injury with normal stromal appearance peripherally (Figs. 7A, 7B). The posterior corneas appeared normal, and peripheral corneal endothelial cells appeared normally distributed on the Descemet's membrane, with some cell reduction centrally, but with a normal appearance (Figs. 7A, 7B). In contrast,

several pathologic features were pronounced in sham DDS–treated eyes. They exhibited corneal epithelial irregularities in the form of either thin, thick, or absent epithelium. In addition, severe anterior stromal scarring, stromal thickening and edema, were evident (Figs. 7C, 7D), accompanied by increased numbers of immune cells infiltrating the cornea, and anterior corneal NV (Figs. 7C, 7D, red arrow). Sham DDS–treated eyes exhibited almost complete loss of endothelial cells throughout the cornea (central and peripheral) (Figs. 7C, 7D—insets), as compared to anti-VEGF DDS–treated eyes that retained endothelial cells (Figs. 7A, 7B—insets). Retrocorneal fibrous membranes (RCFM) were also seen in sham DDS–treated eyes (Fig. 7D, black arrow) but were not seen in the anti-VEGF DDS–treated eyes.

Additional H&E analysis was performed on cross-sections of the DDS and its surrounding conjunctival tissue to evaluate for device tolerance. Eyes treated with anti-VEGF DDS, as well as the eyes treated with the sham DDS, had features of a foreign-body granulomatous reaction within the DDS porous network (Figs. 8A, 8B). Multinucleated giant cells were visible within the pores of the DDS network. Lymphocytes were clustered near the interface between the anti-VEGF DDS and the host conjunctiva with some clusters residing deep within the DDS (Fig. 8A) and with a few small clusters of foamy macrophages present near the interface (Fig. 8A—inset). Importantly, no capillaries were present inside the anti-VEGF DDS at three months, confirming a long-term antiangiogenic effect (Fig. 3A). As in the anti-VEGF DDS, the sham DDS displayed multinucleated giant cells within the DDS porous network (Fig. 8B). Deep inside the DDS, a few lymphocyte clusters were observed in some of the explants. Fewer lymphocytes were present at the interface (Fig. 8D), and capillaries were found inside the DDS containing red blood cells enveloped in the lumen (Fig. 8D).

Anti-VEGF Drug Delivery to the Retina for Three Months Using the DDS and Suppression of Retinal VEGF Expression After Injury

Anti-VEGF mAb was also detected in the retinas (outer limiting membrane, inner/outer photoreceptor segments) three months after DDS implantation (Figs. 9A, 9B), indicating continuous drug permeation to the posterior segment of the eyes over three months of implantation. Anti-VEGF DDS treatment led to nearly 100% inhibition of retinal VEGF-A expression three months after the injury, and resulted to similar retinal VEGF expression as compared to naïve eyes (uninjured controls). However, sham DDS treated eyes exhibited significantly higher VEGF-A expression at three months as compared to anti-VEGF DDS or naïve control eyes (Figs. 9C–9F).

Discussion

This study demonstrates that a micro-porous drug delivery system (DDS), designed for subconjunctival administration of anti-VEGF antibody, reduces corneal inflammation, abrogates peripheral leukocyte infiltration into the cornea, improves corneal wound healing and re-epithelialization, ameliorates corneal stromal fibrosis, and preserves corneal endothelial cells after ocular injury with alkali. Interestingly, the micro-porous DDS achieves anti-VEGF delivery to the retina for three months, which leads to complete suppression of free VEGF without obvious adverse effects.

The mechanism of drug release from this micro-porous DDS is similar to other diffusive polymeric hydrogel-based drug delivery systems,[31,32] and as described in an earlier paper.[20] Two main conditions govern drug diffusion, the rate of PVA swelling and the rate of water infiltration within the PDMS porous network. Because PDMS is intrinsically hydrophobic, water infiltration and hydration of the PVA is retarded. The initial burst drug release is attributed to rapid hydration of the surface of the DDS which is coated by PVA during fabrication. The first-order release is attributed to passive drug diffusion, driven by the concentration gradient between the PVA and the outer environment and controlled by the hydrophobicity of the porous PDMS. Burst release can be reduced by prehydration of the DDS prior to implantation, whereas the first-order release can be prolonged by either increasing the molecular weight or concentration of the PVA or by decreasing the pore diameter of the PDMS network.

Peripheral immune cells are known to secrete inflammatory mediators, such as TNF-α and interleukin-1β, which adversely affect the wound healing process.[22] Indeed, TNF-α inhibition after ocular injury has been shown to improve corneal re-epithelialization,[21,22,25] reduce corneal scarring, improve endothelial cell survival, and prevent the formation of peripheral anterior synechiae.[5,33–37] In this study, we show that early suppression of corneal NV with anti-VEGF DDS reduces TNF-α expression and $CD45^+$ immune cell infiltration into the cornea, ultimately contributing to long-term improvement in

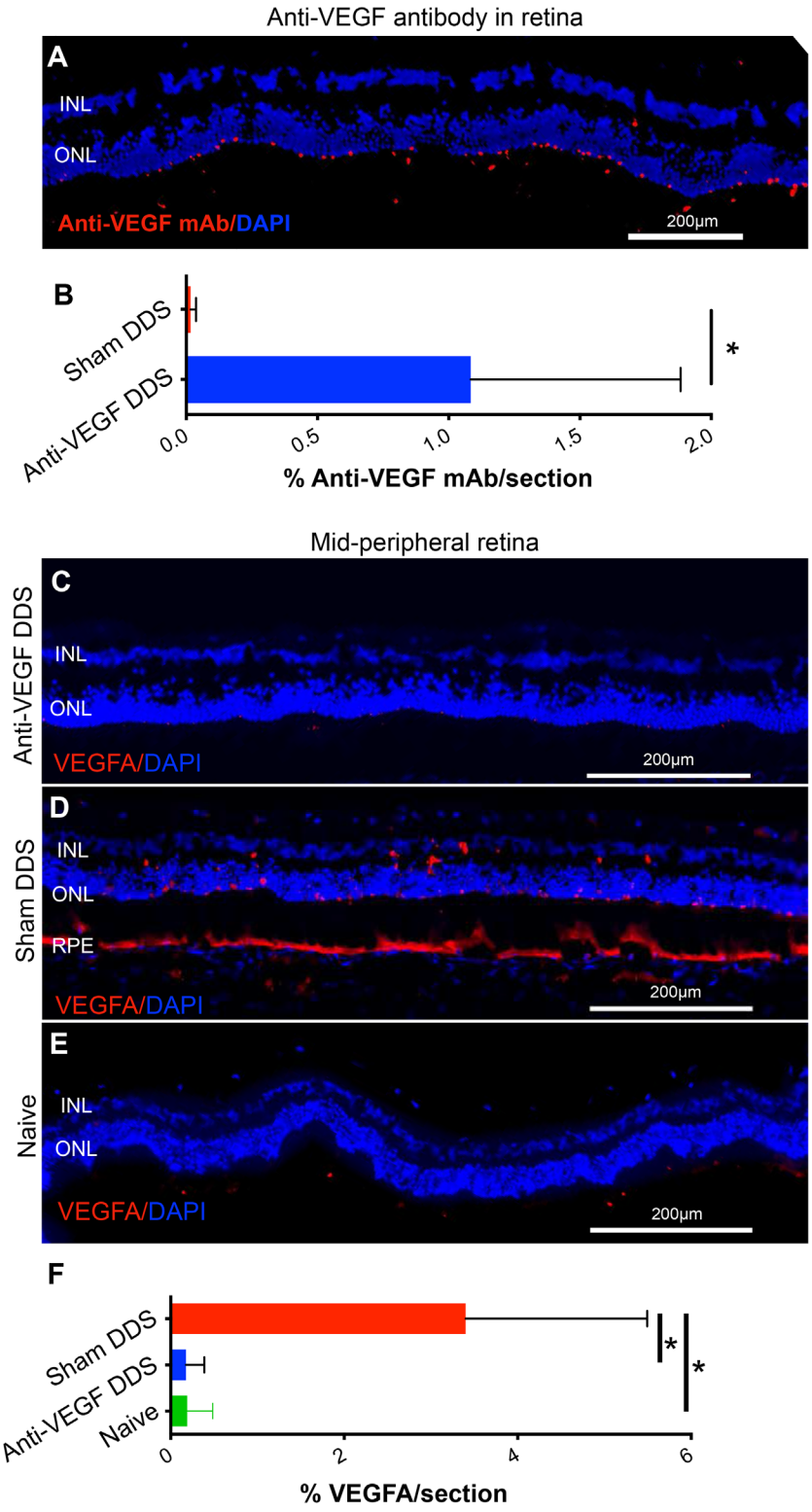

Figure 9. (A) Anti-VEGF DDS delivers bevacizumab to the retina for three months, as evident from scattered anti-IgG staining of small vesicles containing bevacizumab in the outer limiting membrane, and outer/inner photoreceptor segments. Scale bar = 200 µm. Red: bevacizumab detected by anti-human IgG antibody. Blue: DAPI nuclear counterstaining. (B) Quantification of bevacizumab in the retina three months after DDS implantation, (*$P < 0.05$; unpaired *t*-test; n = 3). (C–E) VEGF-A expression in the retina three months after corneal alkali burn. No VEGF-A expression present in retinas of anti-VEGF DDS treated rabbits (C). In contrast, sham DDS–treated rabbits show significant VEGF-A expression in all retinal layers at three months of burn (D). Naïve rabbits had similar VEGF-A expression in retina as anti-VEGF DDS treated rabbits (E). Quantification of VEGF-A expression in the retina, three months after the burn shows significant suppression with anti-VEGF DDS treatment, as compared with sham DDS (F), (*$P < 0.05$; ANOVA test with Tukey's correction; n = 3). (A, C–E) Scale bar = 200 µ m.

corneal re-epithelialization and stromal wound healing as compared with the sham DDS eyes.

Although subconjunctival injection of anti-VEGF antibody achieves adequate corneal penetration,[3,16,38] some previous studies of corneal alkali injury have failed to demonstrate improvement in corneal re-epithelialization after subconjunctival injection of VEGF inhibitor.[38,39] Factors that may have contributed to this inefficacy include the frequency of drug administration, the type of administered inhibitor (small molecule versus antibody), as well as the type and strength of the ocular injury.

Our study demonstrates that anti-VEGF DDS treatment achieves complete inhibition of superior corneal NV for three months, whereas sham DDS treatment results in significant NV during this time frame. However, anti-VEGF DDS treatment does not inhibit inferior corneal NV for more than 10 days. This cannot not be attributed to polymer irritation caused by placement at the inferior bulbar surface because our studies have demonstrated that even superior bulbar placement of the DDS still results in severe inferior corneal NV. We postulate that this is due to the presence of inflammatory cytokine in the tears[40–42] that pool inferiorly due to gravity. In addition, vessel maturation leads to loss of dependency on VEGF signaling, and therefore anti-VEGF therapy gradually becomes less effective.[43] Indeed, Platelet-derived growth factor (PDGF), Placental growth factor (PGF), Fibroblast growth factor (FGF), and Transforming growth factor beta (TGF-β) growth factors facilitate VEGF-independent angiogenesis,[37] and our recent studies suggest that combination treatment with anti-VEGF and anti-PGF inhibitors can prevent superior and inferior corneal NV.

PDMS is bio-inert but not biodegradable.[44] As such, it becomes mildly encapsulated by a thin collagenous membrane with accumulation of lymphocytes and foamy macrophages at its interface, and presence of multinucleated giant cells. This is likely due to foreign body reaction[21] to the implant and antibody antigenicity. This reaction is typical for implantable polymers and can be minimized or reversed with steroid therapy, as previously suggested.[21,44–46] Regardless, these reactions had no bearing on the antiangiogenic efficacy of the anti-VEGF DDS in vivo. This device was designed for the treatment of acute ocular events (e.g., ocular trauma) that typically require one-time therapy.[22] Thus surgical removal of the DDS after completion of the therapy is not necessary but can be performed using explantation surgery, similar to that of glaucoma tube/shunt plate. Redeployment of the DDS is possible by inserting a new implant at a different location, but the number of such attempts are limited due to space restrictions. Our group is working to develop a biodegradable DDS to address the need for repeated applications.

Two additional features were prominent in histopathologic comparisons of the anti-VEGF DDS treated corneas and the sham treated corneas. The first was the degree of corneal stromal scarring and disorganization in the sham-treated group, and the relative preservation of normal corneal stromal architecture in the anti-VEGF–treated group. The second notable feature was the preservation of the corneal endothelial cells in the anti-VEGF–treated group. These beneficial effects of anti-VEGF treatment on the corneal stroma and endothelium represent novel therapeutic outcomes, and suggest a broader than expected impact of anti-VEGF therapy after alkali injury to the cornea.

An additional and important finding of this work is the presence of anti-VEGF antibody in the retina 3 months after implantation of the DDS, which led to a complete inhibition of retinal free VEGF. It is not clear whether retinal VEGF suppression after DDS treatment is due to direct drug diffusion to the retina, or is secondary to the overall improvement of corneal pathology, or even due to the combination of both. However, the presence of bevacizumab in the retina after three months (Figs. 9A, 9B) suggests the likelihood of direct drug effect on retinal VEGF suppression. Previous studies[16,17] have shown that subconjunctival is more efficient than topical administration for macromolecule diffusion to the retina.[16,17] The sclera can absorb macromolecules more efficiently than small molecules and therefore becomes a secondary depot for drug elution to the retina.[16] According to previous studies,[17] subconjunctival administration of a macromolecule (Gd-albumin) achieves two to three orders of magnitude higher concentration in the choroid and vitreous as compared with subconjunctival administration of a small molecule (prednisolone). This is also consistent with our previous anti-TNF-α DDS study, which showed improved drug bioavailability to the retina for three months.[21] Conversely, a single subconjunctival injection of anti-VEGF results in undetectable drug levels in the vitreous at three months.[31,47] To this end, our DDS platform provides the means for efficient long-term delivery of biologic agents to the eye.[20,21] Further studies are required to prove the functional benefit of the DDS for posterior segment angiogenic disorders especially in eyes with physical characteristics closer to the human eye.

In conclusion, sustained, low-dose, delivery of anti-VEGF antibody using the microporous DDS appeared safe and effective in a rabbit model of acute ocular injury. DDS placement in the subconjunctival space reduced corneal NV, stromal scarring,

endothelial cell loss, and inflammation, and improved corneal re-epithelialization following corneal alkali burn. Moreover, it achieved sustained anti-VEGF delivery and subsequent VEGF neutralization in the retina for three months. This treatment modality may prove clinically applicable for the treatment of ocular injuries and neovascular retinal diseases and become a valuable means of delivery of other types of biologic agents to the eye.

Acknowledgments

The authors thank Vassiliki Kapoulea for her contribution to bevacizumab lyophilization and bioactivity validation.

Supported by Boston Keratoprosthesis Fund of Massachusetts Eye and Ear; the Eleanor and Miles Shore Fund; National Eye Institute, and Core Grant no. P30EY003790.

Disclosure: **C. Zhou,** None; **A. Singh,** None; **G. Qian,** None; **N. Wolkow,** None; **C.H. Dohlman,** None; **D.G. Vavvas,** None; **J. Chodosh,** None; **E.I. Paschalis,** (P)

References

1. Bachmann BO, Bock F, Wiegand SJ, et al. Promotion of graft survival by vascular endothelial growth factor a neutralization after high-risk corneal transplantation. *Arch Ophthalmol*. 2008;126:71–77.
2. Chang JH, Garg NK, Lunde E, Han KY, Jain S, Azar DT. Corneal neovascularization: an anti-VEGF therapy review. *Surv Ophthalmol*. 2012;57:415–429.
3. Stevenson W, Cheng SF, Dastjerdi MH, Ferrari G, Dana R. Corneal neovascularization and the utility of topical VEGF inhibition: ranibizumab (Lucentis) vs bevacizumab (Avastin). *Ocul Surf*. 2012;10:67–83.
4. Niederkorn JY, Larkin DF. Immune privilege of corneal allografts. *Ocul Immunol Inflamm*. 2010;18:162–171.
5. Dohlman TH, Omoto M, Hua J, et al. VEGF-trap aflibercept significantly improves long-term graft survival in high-risk corneal transplantation. *Transplantation*. 2015;99:678–686.
6. Lee P, Wang CC, Adamis AP. Ocular neovascularization: an epidemiologic review. *Surv Ophthalmol*. 1998;43:245–269.
7. Chang JH, Gabison EE, Kato T, Azar DT. Corneal neovascularization. *Curr Opin Ophthalmol*. 2001;12:242–249.
8. Shakiba Y, Mansouri K, Arshadi D, Rezaei N. Corneal neovascularization: molecular events and therapeutic options. *Recent Pat Inflamm Allergy Drug Discov*. 2009;3:221–231.
9. Bock F, Konig Y, Kruse F, Baier M, Cursiefen C. Bevacizumab (Avastin) eye drops inhibit corneal neovascularization. *Graefes Arch Clin Exp Ophthalmol*. 2008;246:281–284.
10. Kim SW, Ha BJ, Kim EK, Tchah H, Kim T-i. The effect of topical bevacizumab on corneal neovascularization. *Ophthalmology*. 2008;115:e33–e38.
11. Dastjerdi MH, Al-Arfaj KM, Nallasamy N, et al. Topical bevacizumab in the treatment of corneal neovascularization: results of a prospective, open-label, noncomparative study. *Arch Ophthalmol*. 2009;127:381–389.
12. Koenig Y, Bock F, Horn F, Kruse F, Straub K, Cursiefen C. Short- and long-term safety profile and efficacy of topical bevacizumab (Avastin) eye drops against corneal neovascularization. *Graefes Arch Clin Exp Ophthalmol*. 2009;247:1375–1382.
13. Bock F, König Y, Dietrich T, Zimmermann P, Baier M, Cursiefen C. Inhibition of angiogenesis in the anterior chamber of the eye. *Ophthalmologe*. 2007;104:336–344.
14. Manzano RP, Peyman GA, Khan P, et al. Inhibition of experimental corneal neovascularisation by bevacizumab (Avastin). *Br J Ophthalmol*. 2007;91:804–807.
15. Habot-Wilner Z, Barequet IS, Ivanir Y, Moisseiev J, Rosner M. The inhibitory effect of different concentrations of topical bevacizumab on corneal neovascularization. *Acta Ophthalmologica*. 2010;88:862–867.
16. Ranta VP, Mannermaa E, Lummepuro K, et al. Barrier analysis of periocular drug delivery to the posterior segment. *J Control Release*. 2010;148:42–48.
17. Del Amo EM, Rimpela AK, Heikkinen E, et al. Pharmacokinetic aspects of retinal drug delivery. *Prog Retin Eye Res*. 2017;57:134–185.
18. You IC, Kang IS, Lee SH, Yoon KC. Therapeutic effect of subconjunctival injection of bevacizumab in the treatment of corneal neovascularization. *Acta Ophthalmol*. 2009;87:653–658.
19. Englander M, Chen TC, Paschalis EI, Miller JW, Kim IK. Intravitreal injections at the Massachusetts Eye and Ear Infirmary: analysis of treatment indications and postinjection endophthalmitis rates. *Br J Ophthalmol*. 2013;97:460–465.

20. Robert MC, Frenette M, Zhou C, et al. A Drug Delivery System for Administration of Anti-TNF-alpha Antibody. *Transl Vis Sci Technol*. 2016;5:11.
21. Zhou C, Robert MC, Kapoulea V, et al. Sustained subconjunctival delivery of infliximab protects the cornea and retina following alkali burn to the eye. *Invest Ophthalmol Vis Sci*. 2017;58:96–105.
22. Paschalis EI, Zhou C, Lei F, et al. Mechanisms of retinal damage after ocular alkali burns. *Am J Pathol*. 2017;187:1327–1342.
23. Paschalis EI, Eliott D, Vavvas DG. Removal of silicone oil from intraocular lens using novel surgical materials. *Transl Vis Sci Technol*. 2014;3:4–4.
24. Genentech I. Avastin full prescribing information. 2019.
25. Cade F, Paschalis EI, Regatieri CV, Vavvas DG, Dana R, Dohlman CH. Alkali burn to the eye: protection using TNF-α inhibition. *Cornea*. 2014;33:382–389.
26. Ferrari G, Bignami F, Rama P. Tumor necrosis factor-α inhibitors as a treatment of corneal hemangiogenesis and lymphangiogenesis. *Eye Contact Lens*. 2015;41:72–76.
27. Waterhouse GI, Metson JB, Idriss H, Sun-Waterhouse D. Physical and optical properties of inverse opal CeO_2 photonic crystals. *Chem Mater*. 2008;20:1183–1190.
28. Presta LG, Chen H, O'Connor SJ, et al. Humanization of an anti-vascular endothelial growth factor monoclonal antibody for the therapy of solid tumors and other disorders. *Cancer Res*. 1997;57:4593–4599.
29. Avery RL, Castellarin AA, Steinle NC, et al. Systemic pharmacokinetics and pharmacodynamics of intravitreal aflibercept, bevacizumab, and ranibizumab. *Retina*. 2017;37:1847–1858.
30. Ormerod LD, Abelson MB, Kenyon KR. Standard models of corneal injury using alkali-immersed filter discs. *Invest Ophthalmol Vis Sci*. 1989;30:2148–2153.
31. Lovett ML, Wang X, Yucel T, et al. Silk hydrogels for sustained ocular delivery of anti-vascular endothelial growth factor (anti-VEGF) therapeutics. *Eur J Pharm Biopharm*. 2015;95:271–278.
32. Lim SJ, Lee JH, Piao MG, et al. Effect of sodium carboxymethylcellulose and fucidic acid on the gel characterization of polyvinylalcohol-based wound dressing. *Arch Pharm Res*. 2010;33:1073–1081.
33. Oh JY, Kim MK, Shin MS, Lee HJ, Lee JH, Wee WR. The anti-inflammatory effect of subconjunctival bevacizumab on chemically burned rat corneas. *Curr Eye Res*. 2009;34:85–91.
34. Saravia M, Zapata G, Ferraiolo P, Racca L, Berra A. Anti-VEGF monoclonal antibody-induced regression of corneal neovascularization and inflammation in a rabbit model of herpetic stromal keratitis. *Graefes Arch Clin Exp Ophthalmol*. 2009;247:1409–1416.
35. Sener E, Yuksel N, Yildiz DK, et al. The impact of subconjuctivally injected EGF and VEGF inhibitors on experimental corneal neovascularization in rat model. *Curr Eye Res*. 2011;36:1005–1013.
36. Lee KJ, Lee JY, Lee SH, Choi TH. Accelerating repaired basement membrane after bevacizumab treatment on alkali-burned mouse cornea. *BMB Rep*. 2013;46:195–200.
37. Chen W-L, Chen Y-M, Chu H-S, et al. Mechanisms controlling the effects of bevacizumab (Avastin) on the inhibition of early but not late formed corneal neovascularization. *PLOS ONE*. 2014;9:e94205.
38. Liarakos VS, Papaconstantinou D, Vergados I, Douvali M, Theodossiadis PG. The effect of subconjunctival ranibizumab on corneal and anterior segment neovascularization: study on an animal model. *Eur J Ophthalmol*. 2014;24:299–308.
39. Papathanassiou M, Theodossiadis PG, Liarakos VS, Rouvas A, Giamarellos-Bourboulis EJ, Vergados IA. Inhibition of corneal neovascularization by subconjunctival bevacizumab in an animal model. *Am J Ophthalmol*. 2008;145:424–431.
40. Arafat SN, Robert MC, Abud T, et al. Elevated neutrophil elastase in tears of ocular graft-versus-host disease patients. *Am J Ophthalmol*. 2017;176:46–52.
41. Arafat SN, Suelves AM, Spurr-Michaud S, et al. Neutrophil collagenase, gelatinase, and myeloperoxidase in tears of patients with stevens-johnson syndrome and ocular cicatricial pemphigoid. *Ophthalmology*. 2014;121:79–87.
42. Robert M-C, Arafat SN, Spurr-Michaud S, Chodosh J, Dohlman CH, Gipson IK. Tear matrix metalloproteinases and myeloperoxidase levels in patients with Boston keratoprosthesis type I. *Cornea*. 2016;35:1008–1014.
43. Cursiefen C, Hofmann-Rummelt C, Kuchle M, Schlotzer-Schrehardt U. Pericyte recruitment in human corneal angiogenesis: an ultrastructural study with clinicopathological correlation. *Br J Ophthalmol*. 2003;87:101–106.
44. Belanger MC, Marois Y. Hemocompatibility, biocompatibility, inflammatory and in vivo studies of primary reference materials low-density polyethylene and polydimethylsiloxane: a review. *J Biomed Mater Res*. 2001;58:467–477.
45. Kim SH, Moon J-H, Kim JH, Jeong SM, Lee S-H. Flexible, stretchable and implantable PDMS

encapsulated cable for implantable medical device. *Biomed Eng Lett*. 2011;1:199.

46. Petillo O, Peluso G, Ambrosio L, Nicolais L, Kao WJ, Anderson JM. In vivo induction of macrophage Ia antigen (MHC class II) expression by biomedical polymers in the cage implant system. *J Biomed Mater Res*. 1994;28:635–646.
47. Burgalassi S, Monti D, Nicosia N, et al. Freeze-dried matrices for ocular administration of bevacizumab: a comparison between subconjunctival and intravitreal administration in rabbits. *Drug Deliv Transl Res*. 2018;8:461–472.